Rotor Dynamics and Irregular Wear of Elastic Wheelsets

Thomas Meinders and Peter Meinke

Institute B of Mechanics, University of Stuttgart, D-70550 Stuttgart, Germany

Abstract. High-speed trains in Germany often suffer from vibrations of the car body in the so-called medium-frequency range (30-300 Hz), also known as 100 Hz droning noise. The reason of this unpleasant phenomenon is the development of out-of-round wheels. This paper will discuss the influence of initial out-of-roundness of wheels as well as the influence of wheelset unbalances at high speeds on this wear process. Using a modular approach the model of the wheelset based on the method of flexible multibody systems is coupled to the rail with a complex wheel-rail contact module. In order to account for the long-term wear effects on the wheels the mechanical model is extended by a long-term wear model using a wear-feedback loop in a different time scale. The presented results of wear simulations are subsequently used to discuss the influence of initial out-of-roundness and wheelset unbalances at high speeds on the order and magnitude of developing wear patterns.

1 Motivation

The introduction of the high speed train Intercity Express (ICE) in Germany (1991) has led to new and sometimes only poorly understood problems due to high speed. One of these new problems was easily noticed by passengers due to its loud and disturbing droning noise. The responsible structural vibrations of the car body were excited by out-of-round wheels, which obviously lost their original round shape under the influence of irregular wear. Consequently the changing wheel profiles were causing accelerated wear such that the wheels had to be reprofiled after reaching a critical limit. The characteristic frequency for the excited vibrations of the car body was in the range of 70–100 Hz, which is in the so-called medium frequency range (30–300 Hz).

In order to analyse the rotor dynamics and possible mechanisms for the wear development, an appropriate approach to model flexible bodies in the medium-frequency range has to be selected. Combining the advantages of rigid multibody systems and finite element systems a suitable method is available to account for the first eigenmodes of the wheelset in the questionable frequency range.

2 Flexible Multibody Systems

The method of multibody systems using a minimum set of generalized coordinates has proven to be a very suitable and successful method for the analysis

of constrained mechanical systems, as shown by Schiehlen [18]. In addition to the rigid body approach, where rigid bodies can be connected through massless joints and force elements the extension towards flexible bodies enables the consideration of structural deflections of selected bodies of the multibody system.

The approach to model flexible multibody systems used in this paper is based on the idea assuming large gross motions and superimposed small flexible deformations. For the discretization of the elastic body either local or global shape functions can be used. Due to the flexibility to model even very complex geometric structures, local shape functions (finite element method) have been chosen. The deformation of the structure is described by the modal approach, i.e. through space dependent mode shapes and time dependent modal coordinates, as presented by Kim and Haug [5], Likins [8] and Shabana [19]. The flexible body approach is widely used in vehicle dynamics, see e.g. Claus and Schiehlen [2] and Ambrósio and Gonçalves [1].

2.1 Kinematics and Dynamics

The rigid body motion of a flexible body can be described by introducing a moving reference frame subject to large translational and rotational motions. The position of the reference frame j is then given by the position vector $\mathbf{r}_j(t)$ and the rotation matrix $\mathbf{S}_j(t)$ relative to an inertial frame, see Fig. 1.

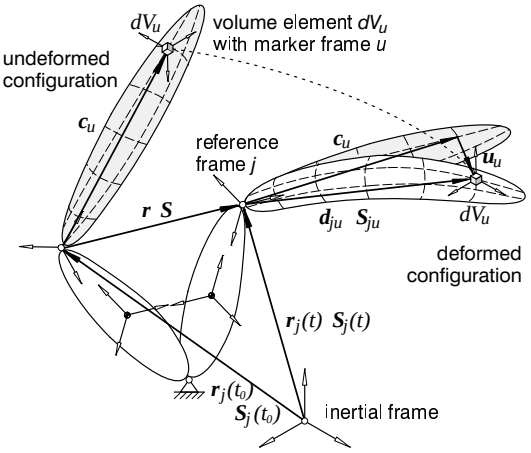

Fig. 1. Definition of deformation and reference vector

The elastic deformations of the body, considered to be small, are described by a displacement vector $\mathbf{d}_{ju}$ and a rotation matrix $\mathbf{S}_{ju}$ linearized with re-

spect to the reference frame. The position of a volume element dV_u relative to the reference frame j is given by

$$\mathbf{d}_{ju}(\mathbf{c},t) = \mathbf{c}_u + \mathbf{u}_u(\mathbf{c},t) \;, \tag{1}$$

where $\mathbf{c}_u$ indicates the position of the marker frame u in the undeformed position and $\mathbf{u}_u(\mathbf{c},t)$ for the displacement field.

In order to minimize the number of degrees of freedom of the system, a modal reduction is used. Thus the displacement field $\mathbf{u}$ is described by a linear combination of a time invariant translational mode shape matrix $\mathbf{\Phi}$, containing selected deformation modes, and the vector $\mathbf{q}$ of generalized elastic coordinates, which are functions of time only:

$$\mathbf{u}_u(\mathbf{c},t) = \mathbf{\Phi}(\mathbf{c})\,\mathbf{q}(t) \;. \tag{2}$$

Assuming only small deformations, the rotation matrix $\mathbf{S}_{ju}$, accounting for the orientation of the marker frame u relative to the reference frame j, is accordingly described as

$$\mathbf{S}_{ju}(\mathbf{c},t) = \mathbf{I} + \tilde{\vartheta}(\mathbf{c},t) \;, \tag{3}$$

where $\mathbf{I}$ denotes a [3x3] identity matrix and $\tilde{\vartheta}$ a skew-symmetric matrix due to the rotational elastic deformations. The matrix $\tilde{\vartheta}$ is derived from the vector of small rotations $\vartheta = [\alpha\ \beta\ \gamma]^T$. According to (2) this rotation vector can be expressed as a linear combination of a time-invariant mode shape matrix $\mathbf{\Psi}$ and the vector $\mathbf{q}$ of generalized elastic coordinates

$$\vartheta_u(\mathbf{c},t) = \mathbf{\Psi}(\mathbf{c})\,\mathbf{q}(t) \;. \tag{4}$$

As mentioned before the discretization of the elastic body can be accomplished either by using local or global shape functions. The advantage of local shape functions is, that even complex geometric structures can be described. Thus using the finite element method, the translational mode shape matrix (2) can be expressed by

$$\mathbf{\Phi}(\mathbf{c}) = \mathbf{S}^T\mathbf{A}(\mathbf{c})\,\hat{\mathbf{S}}\,\mathbf{B}\,\mathbf{T} \;, \tag{5}$$

where $\mathbf{A}(\mathbf{c})$ is the element shape function matrix, $\mathbf{B}$ is the Boolean matrix describing the assemblage of the finite elements and $\mathbf{T}$ denotes the modal matrix, summarizing the mode shapes of the structure. The matrices $\mathbf{S}$ and $\hat{\mathbf{S}}$ transform the displacements from the element to the reference frame. The rotational mode shape matrix $\mathbf{\Psi}$ is obtained in a completely analogue manner.

Before deriving the equations of motions the absolute position and orientation as well as the absolute velocities and accelerations of the marker frame u attached to the volume element dV_u of the elastic body have to be formulated:

$$\mathbf{r}_u = \mathbf{r}_j + \mathbf{d}_{ju} = \mathbf{r}_j + (\mathbf{c}_u + \mathbf{u}_u) \;, \tag{6a}$$

$$\mathbf{S}_u = \mathbf{S}_j\mathbf{S}_{ju} \;. \tag{6b}$$

The expressions for the absolute velocities and accelerations can be derived using relative kinematics, see Melzer [14]. Applying D'Alembert's principle the equations of motion of a flexible multibody system can be written as

$$\mathbf{M}(\mathbf{y},t)\,\ddot{\mathbf{y}}(t) + \mathbf{k}_c(\mathbf{y},\dot{\mathbf{y}},t) + \mathbf{k}_i(\mathbf{y},\dot{\mathbf{y}}) = \mathbf{q}_f(\mathbf{y},\dot{\mathbf{y}},t)\ , \tag{7}$$

with the mass matrix $\mathbf{M}$, the vector of generalized gyroscopic forces $\mathbf{k}_c$, the vector of stiffness and damping forces $\mathbf{k}_i$, and the vector of generalized applied forces $\mathbf{q}_f$. The generalized coordinates of the system are assembled in the vector $\mathbf{y}$, with the vector of the rigid body motion $\mathbf{y}_r$ and the vector of elastic coordinates $\mathbf{q}$ as sub-vectors, such that

$$\mathbf{y}(t) = \left[\mathbf{y}_r(t)\ \mathbf{q}(t)\right]^T\ . \tag{8}$$

Various volume integrals have to be evaluated to obtain the mass matrix. Since small deformations are assumed, these volume integrals can be expanded into a Taylor series of elastic coordinates up to first order. The coefficient matrices of the Taylor series, the so-called shape integrals, are calculated by numerical integration. Since the shape integrals are independent of time, they can be computed prior to time integration by pre-processing. A detailed description of this approach can be found in Melzer [14] and Piram [16].

2.2 Procedure of a Dynamic Analysis for a Flexible System

The procedure of the dynamic analysis of a flexible system is presented in Fig. 2. Starting with the definition of the mechanical model of an engineering system, the elastic parts of a multibody system are discretized using a finite element software, e.g. ANSYS [17]. The resulting data for the mass and stiffness matrix as well as the user-selected eigenmodes of the elastic body is used in a preprocessor, e.g. FEMBS [22] in order to compute the shape integrals describing the elastodynamical behaviour. To gain a maximum of software interoperability, these terms are saved in a standardized format (SID). The equations of motion can be computed by a multibody system code, e.g. NEWEUL [7]. Reading the input-file defining the topological structure of the multibody system and the SID-file containing the information about the elastic body, NEWEUL yields mixed symbolic-numerical equations. The simulation of the system can finally be carried out using standard time integration techniques.

3 Modeling of Rotating Wheelsets

The first step in creating a simulation tool to investigate the development of out-of-round wheels is to set up an appropriate mechanical model of the

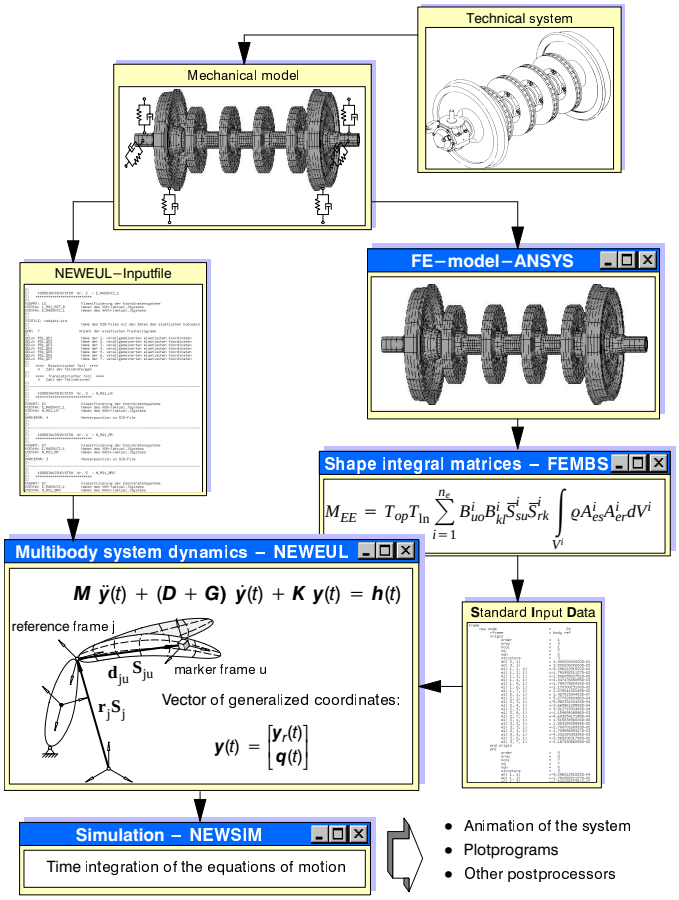

Fig. 2. Procedure of a dynamic analysis of a flexible system

wheelset. Following the procedure exposed in Fig. 2, the essential steps to model the wheelset type BA 14 of the Deutsche Bahn AG, which is the commonly-used wheelset for the German high-speed train ICE 1, are described in the following subsections.

3.1 FE-Model of the Wheelset

The symmetry of the wheelset equipped with altogether 4 disk-brakes is used for the description of the discretized structure by the finite element software ANSYS [17]. In order to gain a maximum of flexibility, the geometric shape of the wheelset is characterized by a set of 54 geometric parameters, as described by Meinders [10]. The 3D finite element structure is generated by rotating a 2D mesh of the wheelset as explained by Meinders [11]. The elements used in this model are SOLID73 from the ANSYS library which provide 6 degrees

of freedom for each of the 8 nodes. This is an important requirement for the later use of the finite element data in the flexible multibody system.

Requirements due to the Rotation of the Reference Frame

The connection between the finite element model of the wheelset and the description of the rigid body model (springs, dampers, bogie coach, rail, etc.) is achieved by a limited number of so-called marker frames u, as shown in Fig. 1. The information about the flexible properties of the body in terms of shape integral matrices is only provided for these selected marker nodes of the finite element model. The reason for this reduction is to keep the size of the overall model and thus the computation time in reasonable limits.

In case of a rotating wheelset the rotation itself is described by a reference frame which is located in the middle of the wheelset on its centerline. Therefore, each node of the structure that is not located on the centerline will rotate with the reference frame with respect to the inertial frame. This can be easily avoided for the interconnecting marker nodes of the primary suspension as well as the marker nodes later needed for the modeling of unbalances by choosing nodes lying directly on the centerline.

The essential wheel-rail contact of the wheelset with its forces and moments is acting on the wheel surface. Therefore, it is not feasible to select one specific node from the surface of the wheels finite element structure since those nodes are rotating relative to the inertial frame.

Realization of the Non-Rotating Wheel-Rail Force

The modeling challenge to realize a non-rotating wheel-rail force acting on the surface of the wheel can be resolved using the following important property of the wheelset: The eigenmode analysis of the FE-structure for the unsupported wheelset (see Fig. 4) as well as for the supported case showed that the wheel-rim has no significant deformation in the frequency range of 0–300 Hz. Thus, the wheel-rim can be treated as a rigid body for the investigation in the medium frequency range.

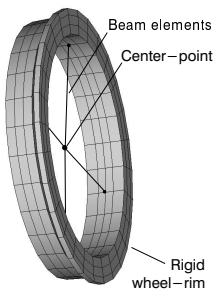

Fig. 3. Center-point

Using this property of the wheel the degrees of freedom of the wheel-rim elements are constrained and supplemented by four also constrained beam elements such that the motion of the rim is represented by the center-point in the middle of the wheel, as shown in Fig. 3. This center-point is subsequently chosen as a marker node. Thus, the necessary wheel-rail contact forces and moments can act on the wheel-rim even though they are applied to the marker in the middle of the wheel.

3.2 Modal Analysis and Selection of the Elastic Coordinates

The first step in analysing and understanding the dynamical properties of the wheelset is a modal analysis. Subsequently the knowledge about the eigenbehaviour in the medium-frequency range is used to select the eigenmodes needed as elastic coordinates in the flexible multibody system.

The resulting eigenmodes of the unsupported wheelset in the frequency range up to 290 Hz are presented in Fig. 4. At a frequency of 82,5 Hz the

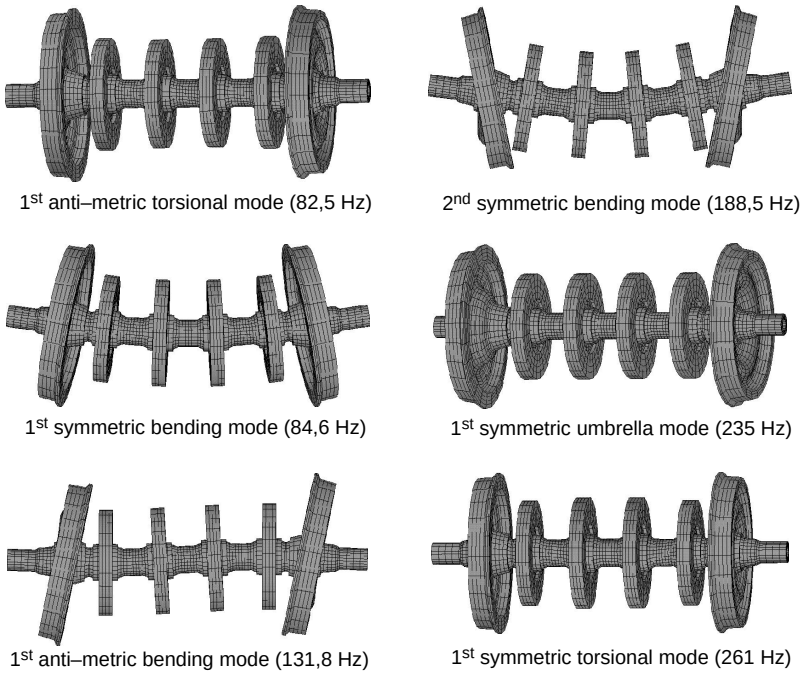

Fig. 4. Eigenmodes of an unsupported wheelset in the frequency range up to 290 Hz

first elastic eigenmode of the wheelset is characterized by a torsional motion of one side of the wheelset against the other with a nodal point between the two inner disk-brakes (1^{st} anti-metric torsional mode). The next two eigenfrequencies at 84,6 Hz are the 1^{st} symmetric bending mode in vertical and horizontal direction. At this low frequency wheels and disk-brakes obviously still behave as if they were rigid. This is not true any more for the 1^{st} antimetric bending mode at 131,8 Hz. At this frequency the flexibility of the wheel membrane influences the movement of the wheels. This can also be found for the 2^{nd} symmetric bending mode at 188,5 Hz, where wheels and disk-brakes bend in opposite directions. At a frequency of 235 Hz the wheel-rims are moving symmetrically along the wheelsets axis. This eigenmode is therefore called 1^{st} symmetric umbrella mode. The 1^{st} symmetric torsional mode at

261 Hz has four nodal points, where the wheels and inner disk-brakes are moving in the same orientation. The last eigenmode in the frequency range up to 300 Hz is the 1^{st} anti-metric umbrella mode at 296,1 Hz.

Based on the knowledge of the eigenbehaviour of the wheelset an accurate selection of type and number of the eigenmodes taken into account for the inclusions in the flexible multibody system is required. Several simulations with different sets of eigenmodes have shown that the umbrella modes as well as the 1^{st} symmetric torsional mode are not necessary to describe the structural vibrations of the wheelset based on the given boundary-conditions and excitations through unbalances, out-of-round wheels or rail imperfections. As a consequence the following seven eigenmodes are included in the model as generalized elastic coordinates:

- 1^{st} anti-metric torsional mode
- 1^{st} symmetric bending mode (vertical & horizontal)
- 1^{st} anti-metric bending mode (vertical & horizontal)
- 2^{nd} symmetric bending mode (vertical & horizontal)

3.3 Consideration of Static and Dynamic Unbalances

One important parameter for the investigation of the wear development of out-of-round wheels are the unbalances of the wheelset. Thus, the model is prepared for the consideration of static and dynamic unbalances.

Static Unbalances
The magnitude of the static unbalances of the wheels and disk-brakes are based on the regulations of the Deutsche Bahn AG, as described by Meinke and Szolc [13]. According to this the limits for admissible static unbalances

$$U = m\,\varepsilon\,, \tag{9}$$

where m is the mass of the rotating body and ε is the eccentricity (due to manufacturing inaccuracies) with respect to the rotating axes of the rotor are as follows: $U_{wheel} \leq 50\ gm$ and $U_{brake} \leq 16\ gm$.

In the flexible multibody system these static unbalances are modeled with mass-points attached to the corresponding marker frame u of wheels and disk-brakes. The position of the static unbalances corresponds to the mounting regulation by DB AG. As depicted in Fig. 5 the static unbalances of the wheels are mounted opposite to the unbalances of the disk-brakes.

Dynamic Unbalances
Dynamic unbalances can be caused by skew mounted disk-brakes or wheels, an inhomogeneous mass distribution in the rotor of due to measures trying

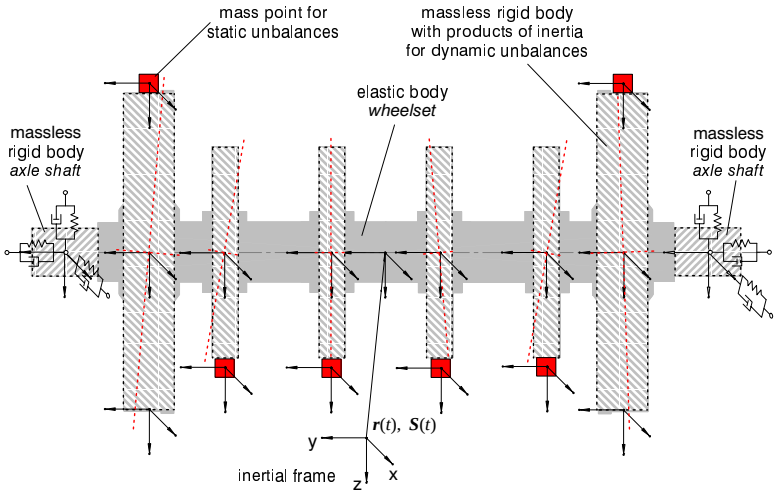

Fig. 5. Consideration of static and dynamic unbalances

to reduce the size of the static unbalances. Dynamic unbalances are characterized by so-called products of inertia such that the matrix for the mass moment of inertia

$$\mathbf{I} = \begin{bmatrix} I_x & 0 & 0 \\ 0 & I_y & I_{yz} \\ 0 & I_{yz} & I_z \end{bmatrix} \tag{10}$$

contains off-diagonal elements, e.g. the product of inertia I_{yz}. In order to consider this in the flexible model of the wheelset it is important to bear in mind that the principal moments of inertia of the wheels and disk-brakes are already described by the shape integral matrices resulting from the fe-description. Consequently the dynamical unbalances are modeled as massless rigid bodies (see Fig. 5), whose matrix for the mass moment of inertia are missing the principal moments of inertia:

$$\mathbf{I} = \begin{bmatrix} 0 & 0 & 0 \\ 0 & 0 & I_{yz} \\ 0 & I_{yz} & 0 \end{bmatrix} . \tag{11}$$

4 Wheel-Rail Contact Module

Railway dynamics are highly influenced by the complex wheel-rail contact situation. Especially for the investigation of wear happening between wheel and rail, a detailed model of this complex contact geometry is essential.

One such detailed model is the wheel-rail contact module of Kik and Steinborn [3], which was originally developed for the use in the multibody system

software MEDYNA. Due to its well-defined input-output structure it was possible to extend the multibody system software NEWEUL/NEWSIM [7] with the ability to describe complex railway systems. A detailed report about the integration of the wheel-rail contact module as a force element in the software package NEWEUL/NEWSIM is given by Volle [21].

4.1 Modular Organization of the Contact Module

The principal modular structure of the contact module is shown in Fig. 6. Based on the current position of the wheel j relative to the rail-head i the

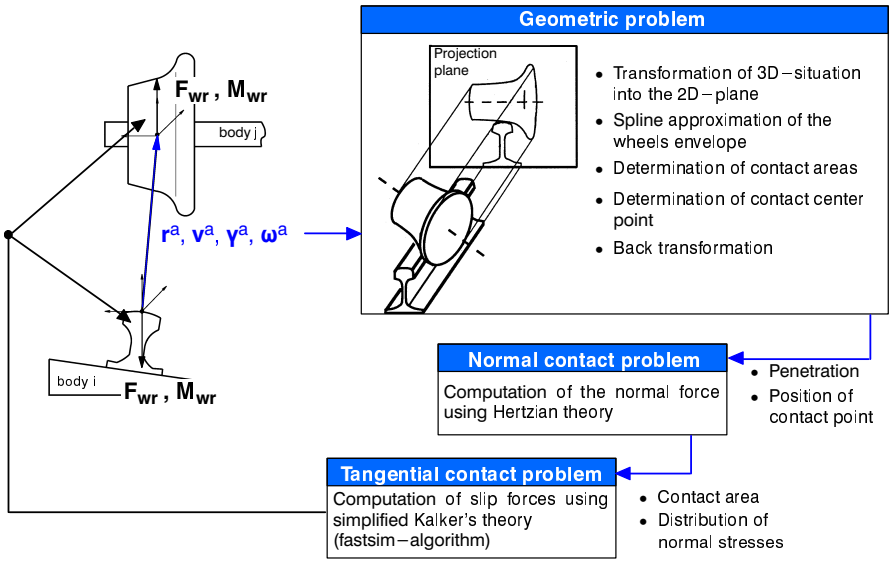

Fig. 6. Modular organization of the contact module

position vector $\mathbf{r^a}$ and the rotation vector $\gamma^{\mathbf{a}}$ as well as the relative velocities $\mathbf{v^a}$ and angular velocities $\omega^{\mathbf{a}}$ serve as the fundamental input parameters for the wheel-rail contact module. Needed for each step of the numerical time integration of the system, the contact module provides the contact forces $\mathbf{F}_{wr}$ and moments $\mathbf{M}_{wr}$ acting between wheel and rail.

As shown in Fig. 6 the contact module is split up into three parts that need to be completed in order to obtain all data for the given contact situation:

Geometric Problem

The contact module enables the use of different spline approximated profiles for wheel and rail. The profiles used for the simulations presented in this paper are UIC60 and S1002. Based on the given relative position of the wheel

relative to the rail the 3D contact geometry is transformed into a 2D plane as shown in Fig. 6. Consequently the contact zones and contact points can be determined. Finally the information obtained from this 2D contact situation is transformed back onto the 3D bodies of wheel and rail. The output data obtained from the geometric part of the contact module are essentially the number and position of the contact points, the resulting penetrations in the contact points and the angles of contact.

Normal Contact Problem
The second part of the contact module, the normal contact part, uses the values of the half-axes of the ellipses and the penetration to compute the normal forces based on Hertzian Theory.

Tangential Contact Problem
Finally the tangential contact part of the module computes the tangential forces, twisting moments as well as the slip values. The contact theory used in this part of the model is Kalker's simplified theory, also often referred to as the FASTSIM algorithm.

4.2 Varying Wheel Radii During Time Integration

One important requirement for the use of the wheel-rail contact module is the possibility to describe varying wheel radii depending on the present angular position of the wheel. Since the focus of the wear investigation requires these radii to change over time the radius $r_j(\varphi)$ has yet to be another input value to the contact module.

As depicted in Fig. 7 the local coordinate system for the definition of the

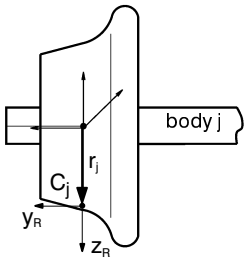

Fig. 7. Definition of wheel profile and wheel radius

wheel profile C_j is not laying in the middle of the wheel, but in the wheels profile itself. By changing the size of the radius $r_j(\varphi)$ the wheels profile in its locally defined coordinate system C_j is changed as a whole.

5 Long-Term Wear Model

The main focus of this paper is the investigation of the wear process of the wheelset. One aspect of this is to determine the amount of mass loss caused by the contact forces and slip values. In order to describe this complex wear process, quite a number of different wear models have been developed, see Kim [4], Specht [20] and Zobory [23]. The wear hypotheses and model for the mass loss used in this paper is presented in Sect. 5.1.

The second part of the wear model is dealing with the long-term effects of the wear. It is therefore necessary to introduce a feedback loop, such that the changing wheel profile is influencing the contact situation between wheel and rail. This influence, often also referred to as long-term behaviour, is happening on a very long time scale that is not accessible through direct time integration.

5.1 Wear Hypothesis and Model for the Mass Loss

The wear model developed for the use together with the contact module from Sect. 4 is based on the following assumptions, see Meinders [12] and Luschnitz [9]:

- The amount of mass loss is proportional to the frictional power (hypothesis of frictional power)
- The wear factor k distinguishes between mild and severe wear
- The frictional power is determined through the contact forces acting in the direction of slip
- Twisting moment and slip are not considered for the calculation of frictional power
- The wear reduces the radius uniformly over the profiles width. It does not change the form of the wheel profile

As mentioned above, the presented wear model is based on the hypothesis, that the loss of material Δm due to wear is basically proportional to the friction work W_R

$$\Delta m = k\, W_R \,. \tag{12}$$

The proportional factor k in (12) is not the same though for all values of frictional power. In fact measurements described by Krause and Poll [6] have shown that the wear factor k is suddenly increasing to a much higher value when a certain frictional power based on the contact area is reached. To reflect this characteristic also shown in Fig. 8, the wear model is distinguishing between mild and severe wear using the following wear parameters:

$$k = \begin{cases} 7 \cdot 10^{-10}\, \frac{kg}{Nm} & : \quad \frac{P_R}{A} \leq 4 \cdot 10^{-6}\, \frac{W}{m^2} \quad \text{mild wear} \\ 2.1 \cdot 10^{-9}\, \frac{kg}{Nm} & : \quad \frac{P_R}{A} > 4 \cdot 10^{-6}\, \frac{W}{m^2} \quad \text{severe wear} \end{cases} . \tag{13}$$

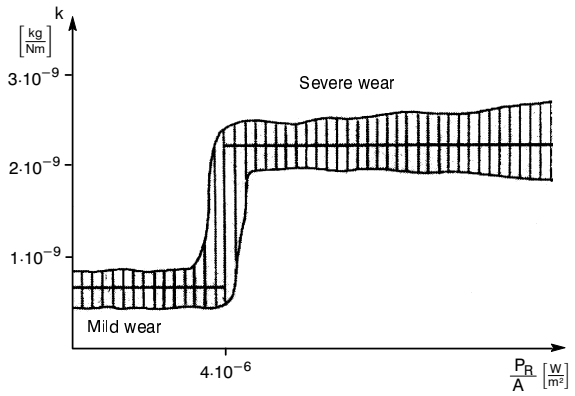

Fig. 8. Wear factor k as a function of frictional power per contact area $\frac{P_R}{A}$ $[\frac{W}{m^2}]$

The physical explanation for this sudden increase of the wear parameter k is also given by Krause and Poll [6]: The material surface of the wheels consists of a thin so-called white-itching layer, which shows a higher resistance against wear than the underlying base material. This white-itching layer is transformed out of the base material due to the wear induced impact. As long as there is an equilibrium between the buildup of the white-itching layer and the abrasive effects of wear reducing this layer, this is considered as mild wear. As soon as the white-itching layer vanishes due to higher frictional power, the much less wear resistant base material is exposed to the wear. This is consequently considered as severe wear.

As mentioned above the frictional power P_R is determined through the contact forces $\mathbf{F}$ acting in the direction of slip $\boldsymbol{\nu}$, that is

$$P_R = \mathbf{F}\boldsymbol{\nu} \; . \tag{14}$$

In order to obtain the changing wheel radius $\Delta r(\varphi)$, the following relations with ρ as the density of the wheel material and A_i as the size of the contact area during the time interval t_i can be written as:

$$\begin{aligned} \Delta m &= \rho \, \Delta V \\ &= \rho \, A_i \, \Delta r(\varphi) \qquad (15) \\ A_i &= \Delta U \, b_i \; . \qquad (16) \end{aligned}$$

Hence, the changing wheel radius $\Delta r(\varphi)$ can be expressed as

$$\Delta r(\varphi) = \frac{\Delta m}{\rho \, b_i \, \Delta U} \; , \tag{17}$$

with b_i and ΔU denoting the width and length of the contact area, as also illustrated in Fig. 9.

Finally, if the wear hypotheses from (12) is used as well as the expression for the length of the contact zone during Δt, that is $\Delta U = V_0 \, \Delta t$ with V_0

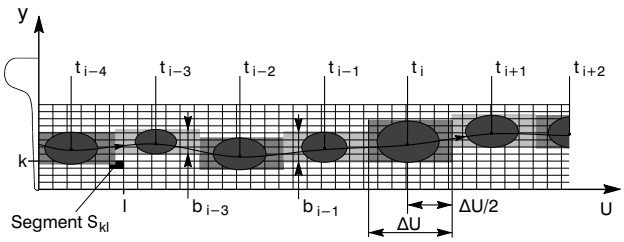

Fig. 9. Distribution of wear over the discretized wheel surface

as the longitudinal speed of the wheelset, the change of the radius for the segment S_{kl} of the discretized wheel surface can be expressed as

$$\Delta r_{kl} = \frac{k\ P_R}{\rho\ b_i\ V_0}\ . \tag{18}$$

5.2 Feedback of Worn Profiles in the Sense of Long-Term Wear

The changing profiles of the wheels, that are slowly losing their original shape due to wear, will influence the dynamics of the system. Therefore, it is important to close the feedback-loop as shown in Fig. 10, such that the changing wheel-radius is used by the contact module.

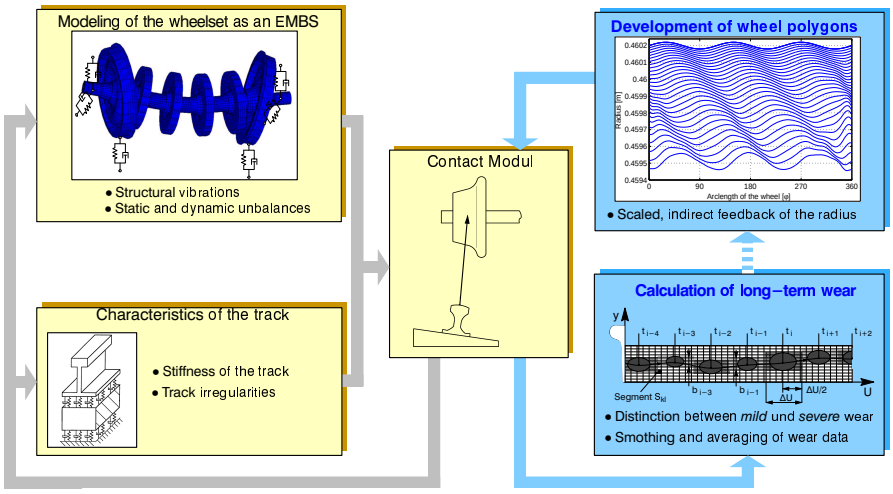

Fig. 10. Feedback-loop of the long-term wear model

In reality the observed phenomenon of developing out-of-round wheels normally takes about 100.000 km in order to show measurable amplitudes of the wheel radius (e.g. $\Delta r = 0,3\,mm$). Even recent computers are not able

to simulate the presented model of the wheelset for a corresponding period of time of presumably weeks or months. Thus it is necessary to introduce a time lapse for the occurring wear. The scaling factor $c_w = 10.000$ is enabling wear simulations with relevant amplitudes of the radius, such that the effects of out-of-round wheels on the dynamics of the system can be studied.

The disadvantage of the amplification of the wear is though, that single wear effects gain an undesirable impact. In order to balance the impact of those effects, the changed radii of the wheels are made available to the contact module in terms of an indirect feedback. This is achieved by accumulating the occurring wear for a number of revolutions $\bar{n} = 10$.

6 System and Wear Behaviour of Elastic Wheelsets

Investigating the behaviour of an ICE 1 wheelset equipped with altogether four disk-brakes, the following aspects are of particular interest: Compared to conventional wheelsets of rail vehicles traveling at lower speed the ICE 1 wheelset is exposed to very high rotational speeds. This is particularly interesting since the moments of inertia considerably increased after adding the four disk-brakes to the wheelset axle. Therefore, it is interesting to investigate whether the wheelset running at high speeds should be treated as a rotor, see Sect. 6.1.

The essential question of this paper is the analysis of the long-term wear development due to different excitations. It is well known, see Morys [15], that even new wheelsets do not have a perfectly round shape, but already show some characteristics of out-of-round wheels. Thus the influence of such initial out-of-roundness is analysed in Sect. 6.2.

Another form of excitation possibly effecting the dynamics and consequently the wear development of the wheels are the unbalances already mentioned in Sect. 3.3.

6.1 Eigenbehaviour of the Wheelset

According to the eigenmode analysis in Fig. 11, the bending modes of the rotating flexible wheelset split into concurrent rotating and counter-rotating eigenmodes. This phenomenon also referred to as bifurcation of the eigenfrequencies clearly shows the characteristic behaviour of an elastic rotor. It is also clear from Fig. 11, that the torsional mode is independent from the rotational frequency. The speed corresponding to the rotational frequency range investigated in Fig. 11 is $V = 0 - 300\,km/h$.

6.2 Wear Development due to Initial Out-Of-Roundness

The simulations of long-term wear showing the influence of the order of initial out-of-roundness have all been carried out with a traveling speed of

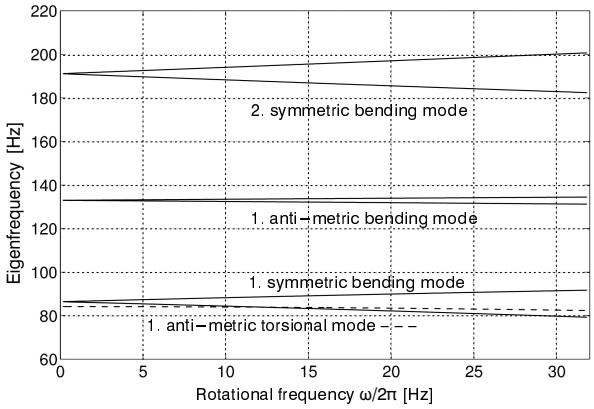

Fig. 11. Bifurcation of the eigenfrequencies over the rotational frequency

$V = 256\,km/h$. The simulation time for all diagrams Fig. 12–15 together with the scaling factor $c_w = 10.000$ (see Sect. 5.2) corresponds to the distance of about 73.600 km. The initial amplitude of the initial out-of-roundness is $\Delta r = 0,02\,mm$. Beside the excitation through initial out-of-roundness there are no other excitations through unbalances or track irregularities.

The initial out-of-roundness shown in Fig. 12 can be caused by excen-

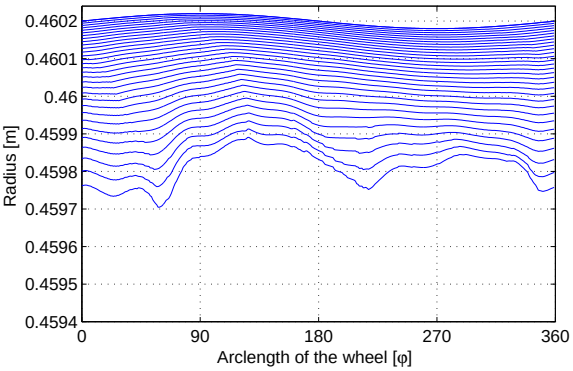

Fig. 12. Influence of initial first order out-of-roundness

tric mounted wheels. Besides the reduction of the overall radius of about $\Delta r \approx 0,4\,mm$ the amplitude is increasing up to $\Delta r \approx 0,2\,mm$. It is clear from Fig. 12, that an initial first order out-of-roundness tends to develop into a second order out-of-roundness.

In contrast to that the second order out-of-roundness as depicted in Fig. 13 is more stable concerning its order. Even though the overall reduction is also

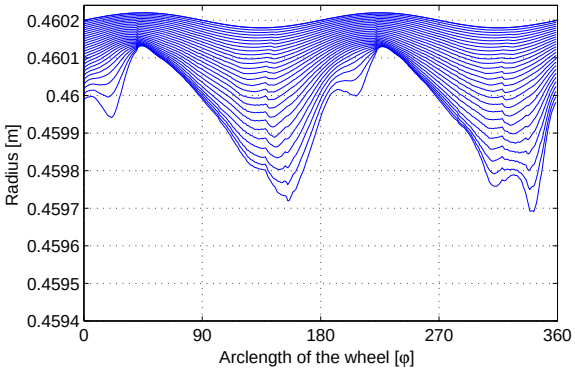

Fig. 13. Influence of initial second order out-of-roundness

about $\Delta r \approx 0,4\,mm$ this wear development leads to an accelerated increase of the amplitude up to $\Delta r \approx 0,4\,mm$.

The highest overall wear of all presented diagrams is obviously caused by the initial out-of-roundness of third order, see Fig. 14. The overall loss of the

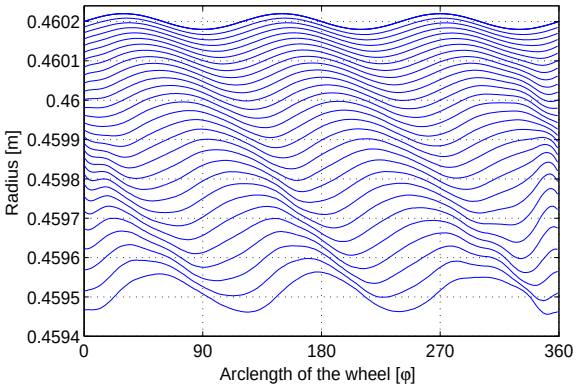

Fig. 14. Influence of initial third order out-of-roundness

radius is $\Delta r \approx 0,7\,mm$, whereas the depth of the amplitude is increasing slowly to $\Delta r \approx 0,1\,mm$.

The fifth order out-of-roundness in Fig. 15 shows similar characteristic as the second order. While the initial shape in relatively stable in shape, the amplitude of the out-of-roundness is increasing up to $\Delta r \approx 0,2\,mm$.

Summarizing the results of the influence of different initial out-of-roundnesses it can be concluded that higher order out-of-roundness tend to be rather stable concerning their shape whereas the first order out-of-roundness leads to second order out-of-roundness.

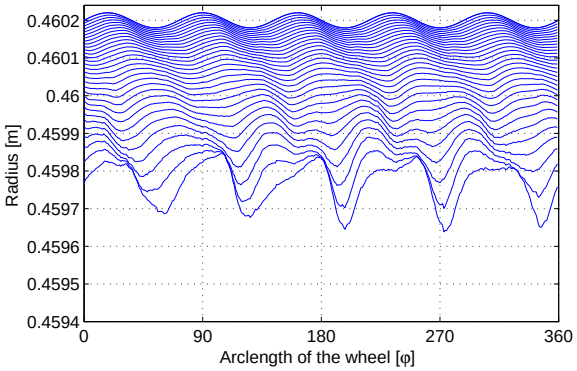

Fig. 15. Influence of initial fifth order out-of-roundness

6.3 Wear Development due to Unbalances

The initial shape of the wheels for investigating the influence of static and dynamic unbalances is a perfectly round wheel. As before the evolving shape of the wheels as shown in Fig. 16 and 17 does correspond to the distance of

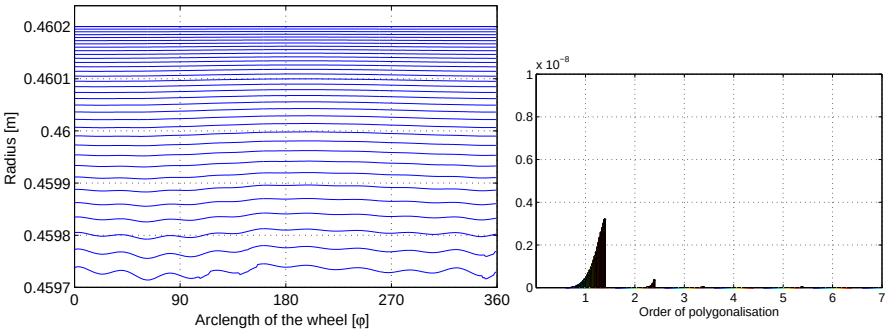

Fig. 16. Wear development due to static unbalances

73.600 km with a speed of $V = 264\,km/h$ and without excitation by track irregularities.

According to the resulting wear development for the excitation with static unbalances in Fig. 16 as well as for dynamic unbalances in Fig. 17 it can be concluded that unbalances do only have a small influence on the wear development compared to the impact of initial out-of-roundness. For both types of unbalances the first order out-of-roundness is emerging. The diagrams on the right hand side of Fig. 16 and 17 show that dynamic unbalances are leading to a three times faster growth of the first order unroundness than the static unbalances.

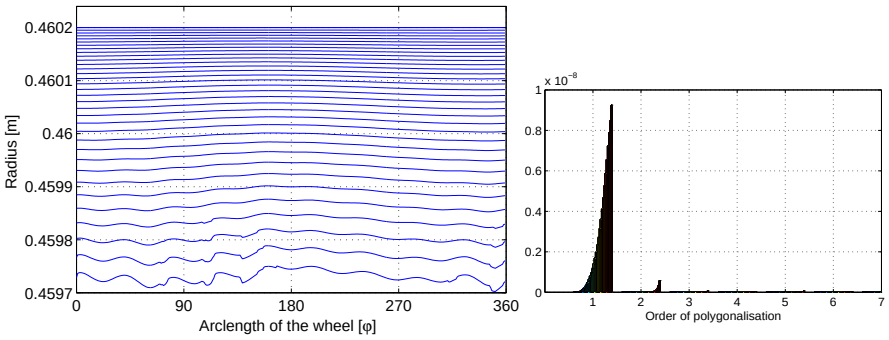

Fig. 17. Wear development due to dynamic unbalances

7 Summary

The approach of flexible multibody systems is used to analyse the rotor dynamics and the developing irregular wear of elastic railway wheelsets. The modeling challenge of a rotating flexible body exposed to the wheel-rail forces is resolved by applying the contact forces to a center-point, which is coupled to the wheel-rim through constrained equations. A modular wheel-rail contact module is integrated in the multibody system software NEWEUL/NEWSIM. In order to account for the appearing wear of the wheels a long-term wear model with a feedback loop for the changing profiles is presented.

According to the eigenmode analysis which results in seven different eigenmodes of the wheelset in the medium frequency range up to 300 Hz, it is essential to consider the possible deformations of the wheelset. The influence of the rotational speed on the bending eigenfrequencies of the wheelset emphasize the relevance of treating the wheelset as a rotor. Initial out-of-roundness prove to have a major impact on the wear development. The growth of the amplitude of all kinds of out-of-roundness is remarkable. Further, the initial shape of second and higher order out-of-roundness are rather stable concerning their shape. Finally static and dynamic unbalances only have a minor influence on the wear development.

Acknowledgment. The financial support of this work under project ME-928/4 by the German Research Council (DFG) is gratefully acknowledged.

References

1. Ambrósio, J. A.C., Gonçalves, J. P.C. (2001) Flexible multibody systems with applications to vehicle dynamics. Multibody System Dynamics, **6**(2), 163–182
2. Claus, H., Schiehlen, W. (2002) System dynamics of railcars with radial- and lateralelastic wheels. Also published in this volume

3. Kik, W., Steinborn, H. (1982) Quasistationärer Bogenlauf - Mathematisches Rad/Schiene Modell, ILR Mitt. 112. Institut für Luft- und Raumfahrt der Technischen Universität Berlin, Berlin
4. Kim, K. (1996) Verschleißgesetz des Rad-Schiene-Systems. Dissertation, RWTH Aachen, Fakultät für Maschinenwesen
5. Kim, S. S., Haug, E. J. (1990) Selection of deformation modes for flexible multibody dynamics. Mech. Struct. & Mach. **18**(4), 565–586
6. Krause, H., Poll, G. (1984) Verschleiß bei gleitender und wälzender Relativbewegung. Tribologie und Schmierungstechnik 31, RWTH Aachen
7. Kreuzer, E. (1979) Symbolische Berechnung der Bewegungsgleichungen von Mehrkörpersystemen, Fortschrittsberichte VDI-Zeitschrift, Reihe 11, 32. VDI-Verlag, Düsseldorf
8. Likins, P.W. (1967) Modal method for analysis of free rotations of spacecraft. AIAA Journal **5**(7), 1304–1308
9. Luschnitz, S. (1999) Ein Modell zur Berechnung des Langzeitverschleißes bei ICE-Radsätzen, Studienarbeit STUD-176 (Meinders, Schiehlen, Meinke). Institute B of Mechanics, University of Stuttgart
10. Meinders, T. (1997) Rotordynamik eines elastisches Radsatzes, Zwischenbericht ZB-94. Institute B of Mechanics, University of Stuttgart
11. Meinders, T. (1998) Modeling of a railway wheelset as a rotating elastic multibody system, Machine Dynamics Problems **20**, 209–219
12. Meinders, T. (1999) Einfluß des Rad-Schiene-Kontakts auf Dynamik und Verschleiß eines Radsatzes, Zwischenbericht ZB-116. Institute B of Mechanics, University of Stuttgart
13. Meinke, P., Meinke, S., Szolc, T. (1995) On dynamics of rotating wheelset/rail systems in the medium frequency range. Dynamical problems in mechanical systems IV, IPPT PAN, Warsaw, 233–244
14. Melzer, F. (1994) Symbolisch-numerische Modellierung elastischer Mehrkörpersysteme mit Anwendung auf rechnerische Lebensdauervorhersagen, Fortschrittsberichte VDI-Zeitschrift, Reihe 20, 139. VDI-Verlag, Düsseldorf
15. Morys, B. (1998) Zur Entstehung und Verstärkung von Unrundheiten an Eisenbahnrädern bei hohen Geschwindigkeiten. Dissertation, Fakultät für Maschinenbau, Universität Karlsruhe
16. Piram, U. (2001) Zur Optimierung elastischer Mehrkörpersysteme, Fortschrittsberichte VDI-Zeitschrift, Reihe 11, 298. VDI-Verlag, Düsseldorf
17. N.N. (2000) ANSYS User's Manual. Ansys Inc., Houston, Pennsylvania
18. Schiehlen, W. (1997) Multibody system dynamics: Roots and perspectives. Multibody System Dynamics **1**(2), 149–188
19. Shabana, A. A. (1989) Dynamics of multibody systems. Wiley, New York
20. Specht, W. (1985) Beitrag zur rechnerischen Bestimmung des Rad- und Schieneverschleißes durch Güterwagendrehgestelle. Dissertation, RWTH Aachen, Fakultät für Maschinenwesen
21. Volle, A. (1997) Integration eines Rad-Schiene-Kontaktmoduls in die Simulationsumgebung NEWSIM, Diplomarbeit DIPL-67 (Meinders, Schiehlen, Meinke). Institute B of Mechanics, University of Stuttgart
22. Wallrapp, O., Eichberger, A. (2000) FEMBS, An interface between FEM codes and MBS codes. DLR. Oberpfaffenhofen
23. Zobory, I. (1997) Prediction of wheel/rail profile wear. Vehicle System Dynamics, **28**, 221–259